Journal of Astronomical Telescopes, Instruments, and Systems

AstronomicalTelescopes.SPIEDigitalLibrary.org

Reflection grating concept for the Lynx X-Ray Grating Spectrograph

Randall L. McEntaffer

SPIE.

Randall L. McEntaffer, "Reflection grating concept for the Lynx X-Ray Grating Spectrograph," *J. Astron. Telesc. Instrum. Syst.* **5**(2), 021002 (2019), doi: 10.1117/1.JATIS.5.2.021002.

Journal of Astronomical Telescopes, Instruments, and Systems 5(2), 021002 (Apr–Jun 2019)

Reflection grating concept for the Lynx X-Ray Grating Spectrograph

Randall L. McEntaffer*
Pennsylvania State University, Department of Astronomy and Astrophysics, University Park, Pennsylvania, United States

Abstract. The Lynx X-ray Grating Spectrograph (XGS) is responsible for providing high throughput and spectral resolution for soft x-ray energies. This instrument will help characterize the formation of galaxies and a large-scale structure in the universe. Such goals require large effective areas, >4000 cm^2, and high resolving power, $R > 5000$, over much of the low-energy band, 0.2 to 2.0 keV. A concept design for the XGS using reflection gratings has the potential to achieve these requirements. The design uses achievable grating parameters, efficient packing of the grating array, and a compact detector layout. The concept is presented along with a detailed discussion of the considerations made in its determination. [DOI: 10.1117/1.JATIS.5.2.021002]

Keywords: diffraction; gratings; x-ray; spectrographs.

Paper 18093SS received Oct. 31, 2018; accepted for publication Dec. 26, 2018; published online Feb. 21, 2019.

1 Introduction

The main scientific contribution of the Lynx X-ray Grating Spectrograph (XGS) is to characterize the diffuse baryonic content in galactic halos and thereby inform formation models to help determine the drivers of galaxy and large-scale structure formation.[1,2] The Lynx XGS will observe 80 sight lines to bright active galactic nuclei (AGN) to reach 1-mÅ sensitivity for absorption lines of OVII and OVIII.[2] This number of sight lines should characterize the halos of galaxies with mass 10^{12-13} M_{Sun} out to their virial radii and beyond for a redshift range of $z = 0$ to 1^2. To accomplish this science goal, the XGS is required to achieve a spectral resolving power of 5000 ($\lambda/\delta\lambda$) and an effective area of 4000 cm^2 over the energy range of 0.3 to 0.7 keV. In addition, the XGS will contribute to detailing galactic feedback from AGN and to the studies of stellar coronal activity and young star accretion, thus requiring sensitivity over the 0.2- to 2.0-keV band.

This paper presents a reflection-grating-based concept for the Lynx XGS. The remainder of this introduction will summarize reflection gratings in the conical mount, current technology development progress in this field, and spectrograph design considerations that must be made when considering the Lynx architecture. Section 2 describes the design of the gratings, the potential layouts for the array of gratings necessary to achieve the effective area requirement, considerations for achieving the resolving power requirement, and a potential configuration for the XGS camera.

1.1 *Reflection Gratings and Conical Diffraction*

An overview of a reflection grating in the conical mount is shown in Fig. 1.[5] Figure 1(a) shows the geometry of conical diffraction,[3] also known as the off-plane mount. In the extreme off-plane geometry, as shown in the figure, the incident light is nearly parallel to the groove direction and at grazing incidence (angle of incidence >88 deg). The reflected image is contained within zero order at angle α in the focal plane. Diffracted light is located at angle β according to the generalized diffraction equation, $\sin(\alpha) + \sin(\beta) = n\lambda/[d \sin(\gamma)]$. Figure 1(b)[4] shows an array of three gratings protruding out of the page with their grooves shown extended down to the focal plane for illustrative purposes. This demonstrates the radial nature that these grooves must have to maintain a constant α across the grating, given that it intercepts a converging beam of light from the telescope. This results in a constant β for a given wavelength and removes grating-induced aberrations to the line spread function (LSF) due to groove period errors. This image also shows the blazed profile that is necessary to preferentially increase diffraction efficiency into the spectral range of interest. This allows for high sensitivity at high dispersion, thus enabling high resolving power concurrently with large effective area. Finally, this image depicts the basic alignment strategy for an array of conical mount gratings; the projection of each grating should overlap at the diameter of the circle in the focal plane that defines the arc of diffraction, and the grooves should converge at the center of this circle. Given all of these considerations, reflection gratings for Lynx must therefore exhibit radial, blazed profiles and be precision aligned to achieve the performance requirements for the XGS.

1.2 *Current Status of X-Ray Reflection Gratings*

Gratings with blazed profiles have been fabricated at Pennsylvania State University's (PSU) Nanofabrication Lab[5] to show the excellent diffraction efficiency allowed by precision blaze angles. Figure 2 shows the diffraction efficiency data[5] obtained from testing in beamline 6.3.2 of the Advanced Light Source at Lawrence Berkeley National Labs. The inset is an atomic force microscope image of the grating surface showing the blazed profile. This is a parallel-groove grating with density of 6275 grooves/mm and blaze angle of ~30 deg. It has been replicated using UV nanoimprint lithography onto a fused silica substrate and coated with 5 nm of Cr and 15 nm of Au for reflectivity. The grating geometry for this test placed the graze angle (90 deg, angle of incidence) at 1.5 deg. The grooves were not oriented exactly parallel to the synchrotron beam

*Address all correspondence to Randall L. McEntaffer, E-mail: rlm90@psu.edu

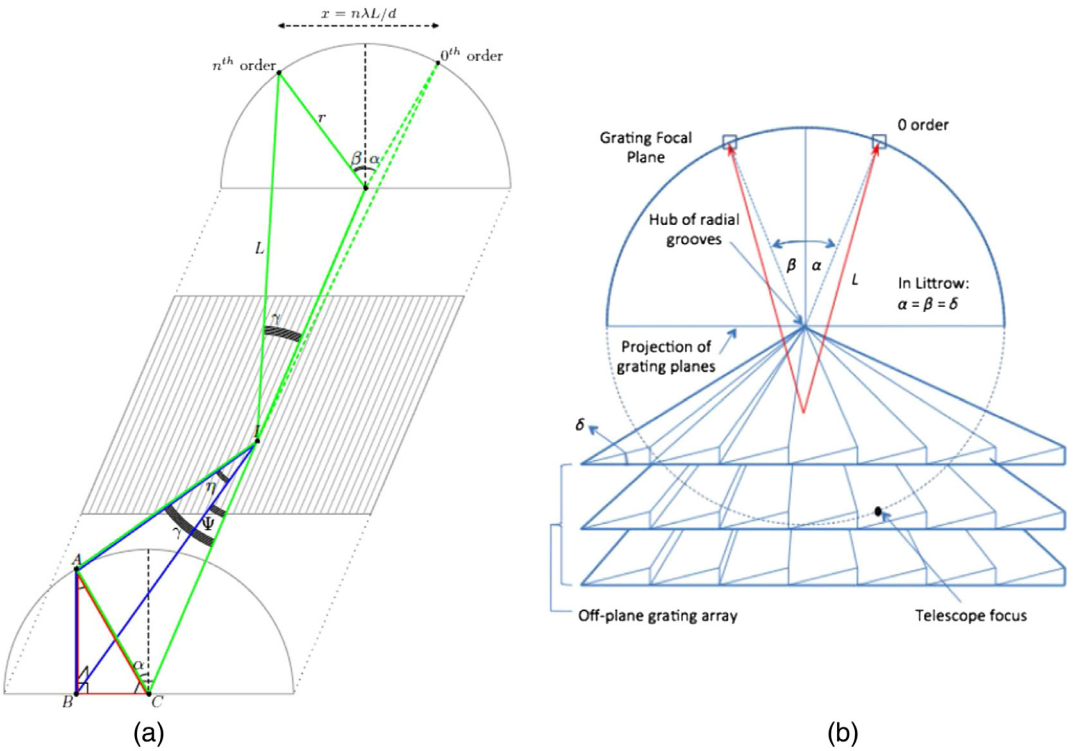

Fig. 1 (a) Geometry of conical diffraction.[3] (b) An array of three gratings is shown projected from the focal plane.[4] Light incident on the gratings will travel to the zero-order position at angle α if reflected, or it will travel to a diffracted order at angle β. The grooves have a blaze angle of δ which provides high-efficiency diffraction, especially when $\alpha = \beta = \delta$. (Figure taken from Miles et al.[5])

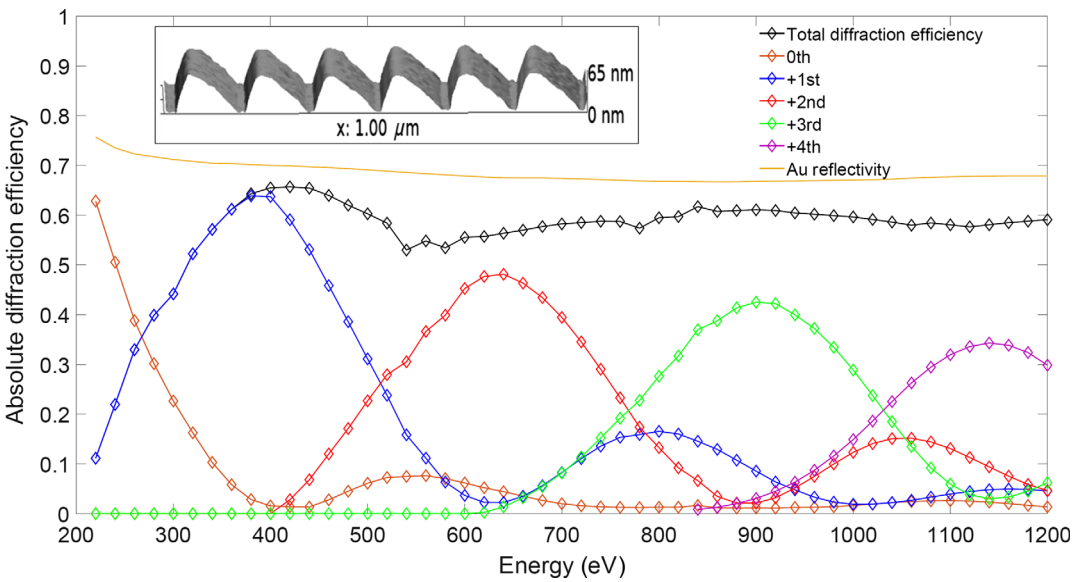

Fig. 2 Diffraction efficiency measurements for a blazed off-plane grating.[5] Inset: atomic force microscope image of the tested grating.

($\alpha = 0$ deg); instead, the grating was rotated about its surface normal (known as a yaw rotation) by 0.7 deg resulting in $\alpha = 25$ deg at the focal plane and $\gamma = 1.7$ deg. This geometry simulates the Littrow configuration, which maximizes efficiency in the blaze direction.

In Fig. 2, the total diffraction efficiency is the sum of all orders and is shown by the black data points. These values are ~90% of the Au reflectivity showing that some light is lost, most likely due to scattering from surface roughness; therefore, some gains could be realized. However, the total efficiency is extremely high and demonstrates some of the largest efficiencies ever measured for gratings over this wide energy band. Furthermore, the single-order efficiencies are high and cover a large range of energy space per order. Early Lynx XGS

concepts baselined 40% diffraction efficiency for the gratings. These results show that this can be easily reached using blazed reflection gratings.

To test resolving power capability, radial profile reflection gratings were fabricated at the PSU Nanofabrication Lab and x-ray tested.[6] The custom groove profile was created using an e-beam lithography tool to write each unique groove individually. The radial profile was transferred into the bulk Si of the substrate to create a laminar profile grating with groove density of 2500 gr/mm. The grating was tested in the converging beam of a silicon pore optic fabricated by cosine measurement systems[7] using the PANTER X-ray Test Facility.[8] The test geometry placed the grating at a graze angle of 1.5 deg and a yaw of 1.6 deg yielding $\gamma = 2.2$ deg and $\alpha = 47$ deg at the focal plane. The tested grating efficiently diffracted out to 30th order using an Al anode electron impact source. The LSFs for the Al Kα1 and Al Kα2 lines are shown in Fig. 3. The data are displayed as a black histogram with error bars.

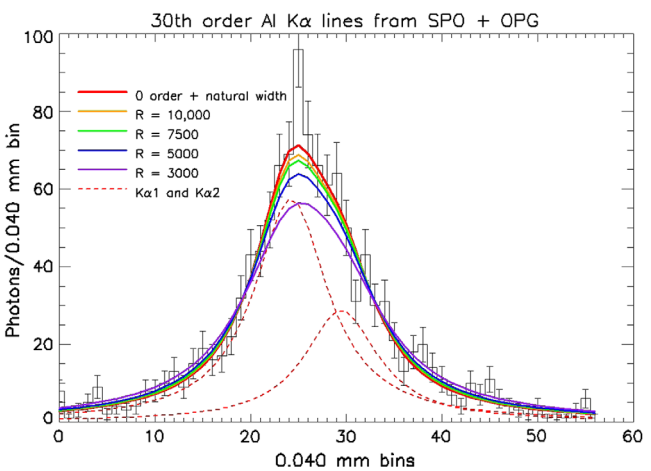

Fig. 3 Resolving power results for a radial profile off-plane grating. Data are shown as the black histogram. The red curve shows a fit to the data using the zero-order image convolved with the natural line widths of the Al Kα_1 and Al Kα_2 lines. Gaussian grating contributions corresponding to certain resolutions are shown in other colors.

The dashed red lines give the expected Lorentzian profiles for the two lines based off the LSF of the zero-order image and the natural line widths.[9] Adding these lines together gives the solid red line and the spectral resolving power limit. Gaussian contributions from the grating can be added to create Voigt profiles of varying width corresponding to resolving powers of 10,000, 7500, 5000, and 3000 as shown by the orange, green, blue, and purple lines, respectively. The telescope-limited resolving power is ~8000 and the statistical difference between the limited case (red line) and resolving power 10,000 is insignificant. The statistical fit to the data becomes poorer as resolving power is lowered from 7500 and lower, thus showing that the result is consistent with a telescope-limited spectrograph. This demonstrates reflection grating performance at least as well as $R \sim 8000$ and that a higher quality telescope with at least as many counts is necessary to probe the grating-limited case. Furthermore, this demonstrates the ability of radially ruled reflection gratings to achieve the $R > 5000$ performance requirement for the Lynx XGS.

Given the recent history of technology development for reflection gratings, they have been vetted at technology readiness level (TRL) 4 by the NASA Physics of the Cosmos Program Technology Management Board. The recent successes in achieving high diffraction efficiency and high resolving power have placed reflection gratings as viable candidates for the Lynx XGS. Ongoing technology development activities, funded by NASA, aim to further grating fabrication studies[5] to make prototypes for Lynx while also investigating alignment strategies[10,11] to fulfill Lynx XGS requirements.

1.3 *XGS Within the Lynx Observatory*

An overview of the Lynx observatory architecture is shown in Fig. 4. This is an exploded view to reveal various components of the observatory. The spacecraft bus and Lynx Mirror Assembly are located at the forward end. The focal length of the telescope is 10 m. The XGS grating array is located just aft of the telescope and can be actuated in and out of the beam depending on the science target of interest. The forward assembly is separated from the aft end by an optical bench. The Integrated Science Instrument Module is located at the aft end and consists of

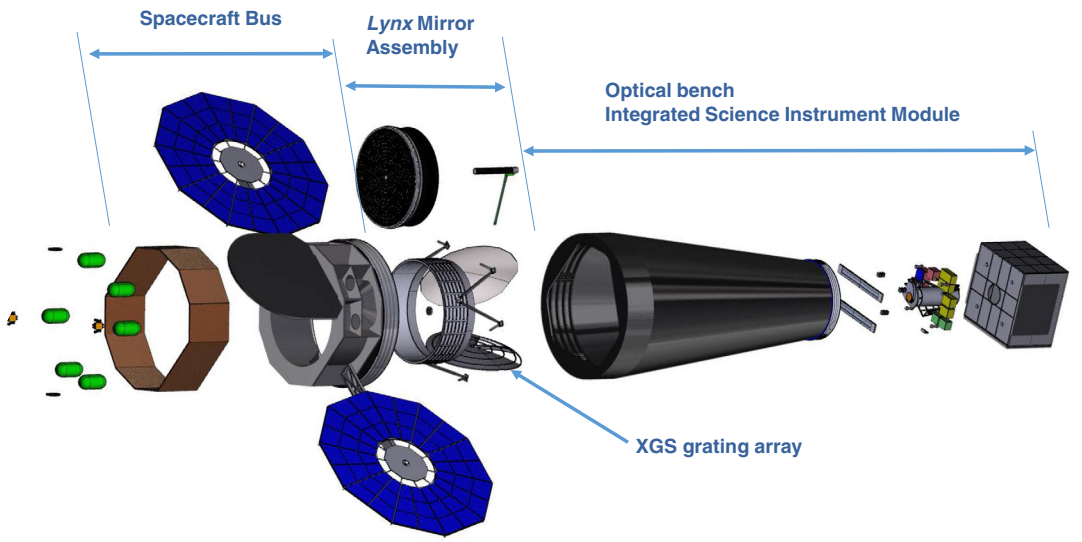

Fig. 4 An exploded view of the Lynx observatory.

the High-Definition X-ray Imager (HDXI), the Lynx X-ray Microcalorimeter (LXM), and the camera for the XGS. There is a selection of papers in this special journal edition describing these and other Lynx instruments and systems.

When designing a reflection grating spectrograph for the Lynx XGS, several conditions and assumptions must be applied. The concept presented here uses this base set of assumptions to identify a starting point for a baseline concept; however, as the observatory design evolves, this XGS concept will evolve as well. First, it is assumed that the telescope will produce a point spread function (PSF) of 0.5-arc sec half-power diameter (HPD). The relative contributions to this PSF, such as figure error or scattering, are not yet known and are therefore not considered. Second, the distance from the XGS to the focal plane, also known as the throw, is assumed to be 9.5 m. Third, the final LSF for a spectral line is assumed to be 1.0-arc sec full width at half maximum (FWHM). Given a 0.5-arc sec telescope, this leaves 0.87 arc sec of grating contribution to the LSF, which could result from factors such as misalignments and period errors. Finally, it is assumed that the key science will be performed with the He-like OVII triplet around 22 Å. For design purposes, performance is optimized at 568 eV. In the case of effective area, the requirement is increased by 10% to 4400 cm^2 to account for unknown factors, such as contamination or unknown structural obscurations.

2 Reflection Grating XGS Design

The following sections describe the design considerations that must be made to formulate a reflection grating concept for the Lynx XGS. These considerations use the assumptions from Sec. 1.3 as initial conditions to determine the grating design, array layout, focal plane layout, and, hence, baseline design for a reflection grating XGS.

2.1 *Grating Parameters*

The grating used to produce the high resolving power results in Fig. 3 has a groove density of 2500 gr/mm. This has therefore been adopted as the initial groove density for consideration for Lynx. Reflection gratings with much higher densities have been written using e-beam lithography,[5] but lower densities lead to lower period error contributions, and therefore, potentially higher resolving power. This requires operating at higher order for a given dispersion, which is only an issue if the detector energy resolution is poor. Combined with the 9500-mm throw, this density gives a dispersion of 0.42 Å/mm. A 1-arc sec FWHM LSF covers a 0.0485-mm width at the focal plane, which is 0.0204 Å wide in wavelength, given the dispersion. Achieving a resolving power of 5000 will therefore occur for wavelengths longer than $n\lambda = 102$ Å. The LSF width also places a constraint on the detector pixel size. The XGS readout is currently being modeled after the design of the HDXI, which has a working pixel size of 16 μm, adequate for the designed LSF. Effective off-plane geometries and reflection efficiencies of typical metallic coatings argue for a graze angle around 1.5 deg (incidence angle of 88.5 deg). Along with the resolving power requirement, this produces a blaze angle around 27 deg, which places efficient diffraction for OVII in fifth order, for example. The blazed grooves will have a radial profile to match the convergence of the telescope.

2.2 *Design Considerations for Effective Area*

The baseline XGS design for Lynx requires that the grating array be actuated in and out of the beam depending on the science target of interest. When the grating array is in the telescope beam, concurrent observations will take place with one of the other focal plane instruments, either the HDXI or the LXM. Therefore, it is important to limit the amount of telescope area occulted by the XGS while still achieving the effective area goal. This also minimizes the mass of the grating array. If the XGS does not cover the entire telescope aperture, then placement of the array should be optimized by considering the effective area of the telescope as a function of radius while also considering potential system impacts such as location of structures, e.g., the actuation mechanism and the contamination door.

The telescope effective area is shown in Fig. 5. These plots use predictions from the baseline Lynx telescope design consisting of 12 shells of polished Si optics. Figure 5(a) shows how the mirror effective area per geometric area varies as a function of the 12 radially spaced shells. The mirror effective area in this case is taken as a sum of effective areas at eight energies that span the XGS band (0.2, 0.4, 0.6, 0.8, 1.0, 1.4, 1.8, and 2.0 keV). This value is then divided by the geometric area of each annular shell to arrive at the y values. This demonstrates that the most effective shells are 4 and 5 (numbering from 1 closest to the center and 12 at the highest radius) followed

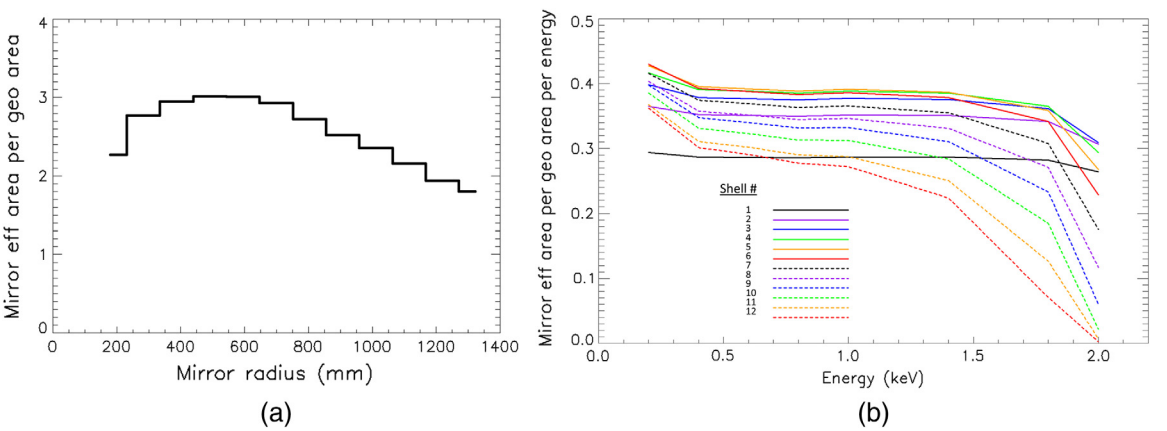

Fig. 5 (a) The mirror effective area per shell, summed over area and divided by the geometric area, as a function of radius. (b) Similar to (a) but now shown as a function of energy.

by 3 and 6, and so on. Even though the outermost radii contribute a large geometric area, the higher relative graze angles lead to poorer reflectivity. In addition, Fig. 5(b) shows the mirror effective area per geometric area, defined in the same way but now displayed as a function of energy and shell. Again, the mid-range shells are the most effective with weighted throughput dropping off for shell 1 and shells >8, especially at higher energy for the latter.

With the telescope area in hand, the throughput of the remaining XGS systems must be accounted for to ensure that >4400 cm^2 can be achieved at 568 eV. Figure 6 plots the various contributions as a function of energy. In Fig. 6(a), curves are shown for throughput of the detector assembly. The contributions include the detector quantum efficiency, 30 nm of directly deposited Al with a 10-nm oxidized layer (Al_2O_3) serving as an optical blocking filter, and 45 nm of Kapton on a 95% transmissive support mesh that serves as a warm contamination filter. The sum of these contributions is shown as the thick black curve. This curve is repeated in the center plot for reference as the dashed line. The solid line in this center plot is the theoretical grating efficiency for the grating design described in Sec. 2.1 as calculated by the PCGrate diffraction efficiency code. The grating efficiency is then reduced by the geometric throughput of the array, which is assumed to be ~81% given realistic support structures. The combination of telescope efficiency, detector efficiency, and grating efficiency then produce a total XGS effective area curve. A coverage factor for the grating array can be added in to enforce a lower limit of 4400 cm^2 at 568 eV. This results in the curve in

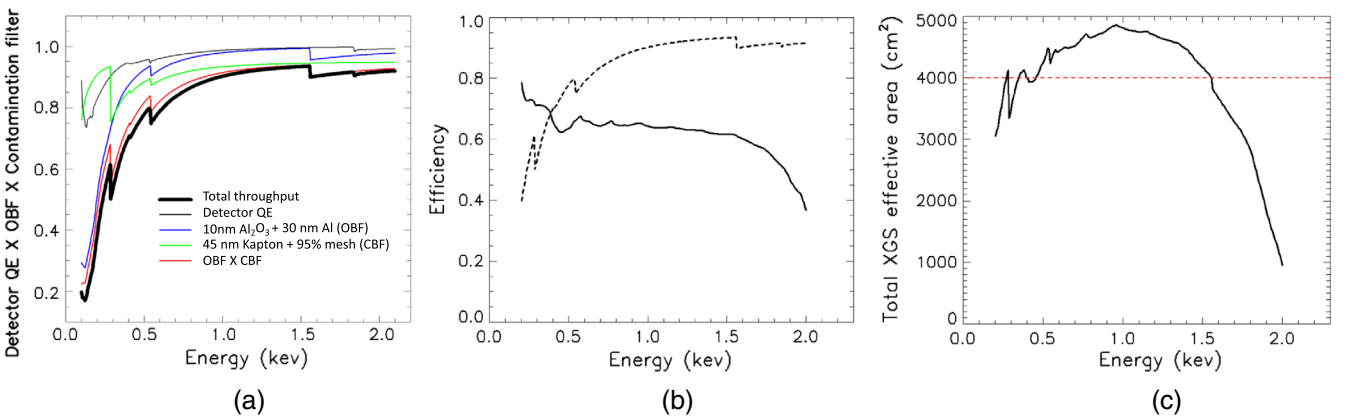

Fig. 6 (a) Throughput curves for the detector assembly. (b) The dashed line is the total detector throughput and the solid line is the theoretical grating diffraction efficiency. (c) The total reflection grating XGS effective area curve. The dashed red line shows the Lynx requirement of 4000 cm^2.

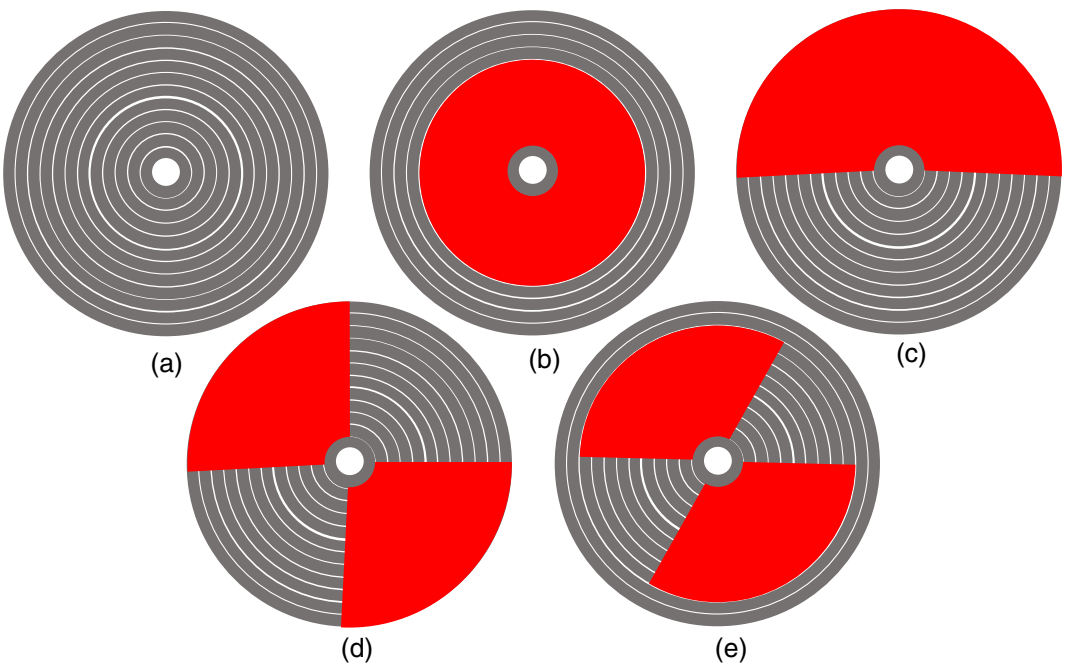

Fig. 7 Potential reflection grating XGS layouts (red) superimposed on the 12 telescope shells. (a) The 12 shells of optics. (b) Optimal grating coverage is shown as the red annulus. (c–e) Alternative grating configurations are shown as red sections. These are slightly less efficient than the configuration in (b), but potentially more practical from a systems standpoint.

Fig. 6(c). In this case, it is assumed that only telescope shells 2 to 12 are utilized, which leads to a coverage factor of 50% (50% unobstructed telescope).

Given the effective area variation over the telescope area, combined with the fact that only approximately half of the telescope needs to be covered, there are several grating array layouts that were considered for the reflection grating XGS (see Fig. 7). Each of these layouts achieve >4400 cm^2 at 568 eV but cover different sections of the telescope to elucidate design considerations for the grating array layout. Figure 7(a) shows the 12 radial shells of the optic, whereas Figs. 7(b)–7(e) show the grating array as red areas superimposed upon the optics. The array in Fig. 7(b) gives the highest unobscured fraction of the telescope (54%), given that it only covers shells 2 to 8, the most effective. However, the mechanical interface between the array and its support structure on the optical assembly will likely be placed at the periphery of the optics, thus making implementation of this array layout difficult, e.g., more structural mass will be required to support the cantilevered array, and this structure will obscure parts of the optic. Therefore, Figs. 7(c) and 7(d) show two options that extend the array to cover shells 2 to 12 resulting in 50% coverage [recall Fig. 6(c)]. This can consist of a continuous 184-deg segment as shown in Fig. 7(c) or two 92-deg wedges as shown in Fig. 7(d). Finally, Fig. 7(e) presents a compromise between Figs. 7(b) and 7(d). In this case, the array coverage is 48% of the telescope (52% uncovered optic) and shells 2 to 10 are utilized. This places array elements closer to the periphery while attempting to minimize telescope coverage. This also starts to demonstrate the flexibility of the array configuration; several reflection grating layouts can achieve the effective area requirement for Lynx, which affords a wide range of options when the final observatory configuration is reached.

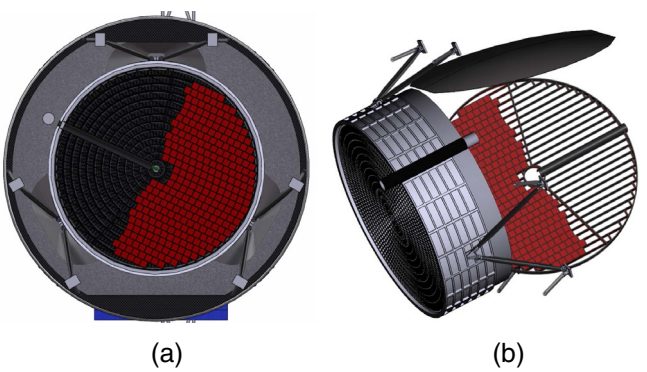

Fig. 8 The reflection XGS relative to Lynx Mirror Assembly. (a) An image of the grating modules, colored red, inserted into the telescope beam as viewed from the focal plane. (b) An isometric view of the optical assembly with the grating array actuated out of the telescope beam.

2.3 *Lynx Reflection XGS Concept*

The continuous 184-deg section for the grating array was considered for the reflection XGS during phase 6 of the NASA's Marshall Space Flight Center Advanced Concepts Office (ACO) design study for Lynx. The grating array is shown relative to the Lynx Mirror Assembly in Fig. 8. In Fig. 8(a), the perspective is along the optical axis from the detector toward the optics. The optics are depicted by the 12 dark gray annuli, and the gratings are shown as red modules each measuring 10×10 cm. The image in Fig. 8(b) shows the grating array actuated out of the telescope beam.

The 184-deg section could be thought of as two 92-deg wedges. A zoom-in on one of the two wedges is shown in Fig. 9 with a potential distribution of grating modules. Each module is depicted by a green box and measures $10 \times 10 \times 10$ cm in volume. This module design is based on reflection grating modules that have been previously fabricated for suborbital rocket missions [Fig. 9(b)]. Given the 1.5-deg graze angle, 0.5–mm–thick substrates, and 100–mm groove length, each module will house 32 gratings. There are 154 modules in this wedge design, which leads to a requirement of 9856 gratings to populate the entire 184-deg section. A similar array architecture was considered during a recent ACO study, and the resulting array mass, including all gratings and array support structures, was ~116 kg.

2.4 *Design Considerations for Resolving Power*

When determining the resolving power performance of a spectrograph, the telescope PSF is often a large contribution to the final LSF. However, knowledge of factors influencing

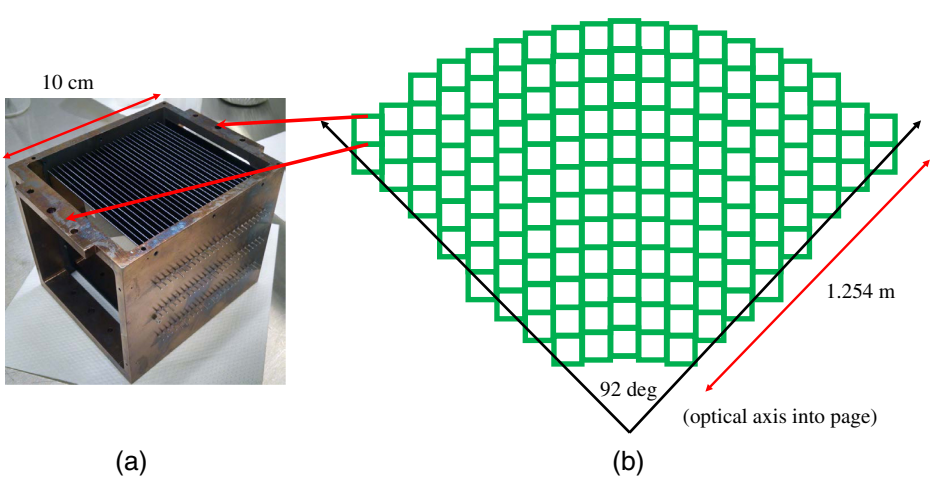

Fig. 9 (a) A grating module layout is shown for a 92-deg wedge of the grating array. Each module is shown as a green square. (b) A zoom-in on one of these squares is shown to the left using an image of an existing module of gratings that was used for a suborbital rocket mission and exhibits similar dimensions.

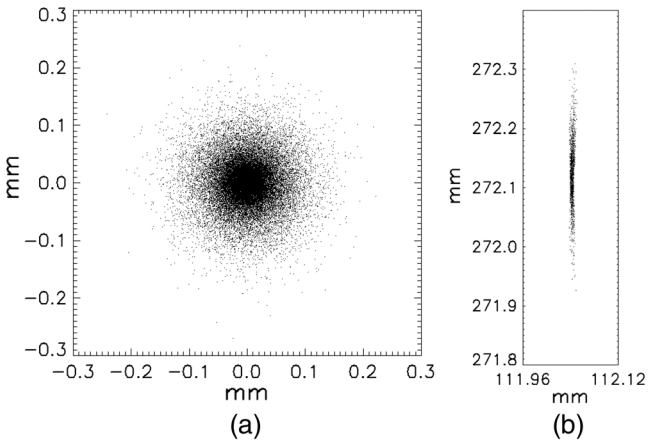

Fig. 10 (a) Focus resulting from a raytrace of the Lynx optics. The HPD is 0.5 arc sec. (b) LSF of fifth-order OVII resulting from one grating module. The HPD is 0.06 arc sec in the dispersion direction (x).

the telescope PSF (e.g., surface roughness, mid-frequency error, and alignment) is necessary for an in-depth analysis of the true LSF given that a single grating samples only a small section of the telescope resulting in a single-grating LSF that can differ depending on which telescope factors are truly dominant. The Lynx telescope is still early in development so knowledge of these factors is extremely limited and a detailed raytrace of their effects on the LSF will provide limited information. Establishing various realistic models of each telescope influence on the spectral resolving power is beyond the scope of the current Lynx XGS study; however, it is important to note that this must be performed later in development when realistic estimates of the telescope contributions can be determined.

Although the above is true, some insight can be drawn from a basic raytrace example. Figure 10(a) shows a raytrace of a scatter-dominated Lynx telescope. This model covers the range of appropriate radii from the 12 shells and has a 10–m focal length. The resulting HPD of the PSF is 0.5 arc sec, per Lynx baseline telescope requirements. Figure 10(b) shows the LSF of fifth-order OVII diffracted from a single module of gratings. The module only samples a small azimuthal range of the telescope, and this subaperturing effect leads to a much narrower LSF in one dimension. The resulting line is not Gaussian but exhibits an HPD of only ∼0.06 arc sec. Therefore, for a scatter-dominated telescope, the subaperturing effect is strong and individual modules produce lines with narrow LSFs. In this case, grating-to-grating and module-to-module alignments are likely to dominate the error budget, i.e., a telescope PSF that can be effectively subapertured will lead to looser grating alignment tolerances.

Maintaining spectral resolving power above 5000 over the 0.2- to 2.0–keV band places constraints on operating order as a function of wavelength. Furthermore, order confusion in the focal plane places an energy resolution requirement on the detector. These considerations, combined with the dispersion of the gratings, result in the wavelengths per order as shown in Table 1. There are no gaps in coverage over the Lynx XGS band, and the resulting energy resolution requirement of 80 eV is obtainable with the current HDXI sensor design. Furthermore, the resulting resolving power ranges from 5000 to 7700 per order, allowing for many wavelength regions of much higher resolving power. The wavelengths per order can be tuned using the blaze angle on the gratings, thus allowing for optimization of resolving power for the most important science wavelength bands of interest; this is a goal for a future Lynx XGS study.

Table 1 Wavelengths per order for the reflection grating XGS design.

Order	Wavelengths (Å)	Order	Wavelengths (Å)
1	102 to 157.2	10	10.2 to 15.72
2	51 to 78.6	11	9.27 to 14.29
3	34 to 52.4	12	8.5 to 13.1
4	25.5 to 39.3	13	7.85 to 12.1
5	20.4 to 31.44	14	7.29 to 11.23
6	17 to 26.2	15	6.8 to 10.48
7	14.57 to 22.46	16	6.375 to 9.825
8	12.75 to 19.65	17	6.0 to 9.247
9	11.33 to 17.47	—	—

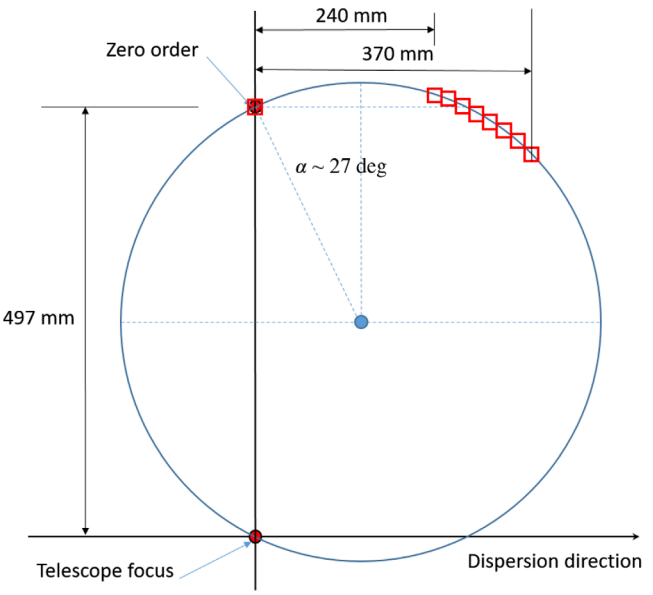

Fig. 11 Potential focal plane sensor layout for the reflection XGS.

The grating geometry and dispersion combined with the $n\lambda$-space order extents in Table 1 lead to the spectral location on the focal plane. Figure 11 shows a potential focal plane layout for this configuration. The modest dispersion range requires only ∼131 mm of detector coverage in the dispersion direction, which can be accomplished with 8 spectral detectors assuming the current HDXI size of 16.384 mm per sensor. These sensors will follow the arc of diffraction, as will the zero-order sensor, which will be used for wavelength calibration. Rotation of the grating array around the optical axis will result in a rotation of this layout about the telescope focus.

3 Conclusion

An initial design for the Lynx XGS based on reflection gratings has been formulated. Reflection gratings operating in the

extreme off-plane geometry can offer high spectral resolving power when the groove profile matches the converging beam of the telescope. Also, blazed grooves on reflection gratings can offer diffraction efficiencies near the theoretical limit. These attributes allow for the formulation of grating array and detector layouts for Lynx.

The reflection grating XGS can achieve >4400 cm^2 of effective area at 568 eV (OVII) while obscuring only 50% of the telescope. This allows for efficient concurrent observations with other Lynx instrumentation, such as the LXM or HDXI. The grating array can be configured in a variety of ways, thus allowing for easy accommodation for potential system impacts or design changes. The azimuthal clocking of the array relative to the observatory also allows some customization on the placement of the diffraction arc at the focal plane. This could be exploited to remedy mechanical interferences in the instrument module.

The current design assumes a final LSF of 1-arc sec FWHM given a 0.5-arc sec telescope HPD. Using this assumption, the design of the grating results in reasonable groove parameters. The grating geometry can then be used to predict the spectral location and extent on the focal plane and, therefore, the detector layout while also determining the relevant order per wavelength and expected resolving power. The latter ranges from 5000 to 7700 per order.

In addition to the ongoing design work, there are several areas of future work for a reflection grating XGS. First, a detailed raytrace of the system is a necessary next step. This raytrace should include realistic contributions to the telescope PSF so that the LSF can be accurately modeled. The raytrace will refine placement of the grating modules within the array and allow for a detailed error budget to be constructed that includes definition of the alignment tolerances. Second, the technology development roadmap will be refined. A current plan exists but may need editing based on potential challenges identified by the detailed raytrace and error budget. Associated with this roadmap, costs associated with technology development leading to TRL 6 need to be assessed. Next, there may exist options for improvements in performance. New fabrication methods are making reflection gratings easier to fabricate, with better resolving power, more efficiency, and greater ease of alignment. Furthermore, when more is known about the telescope PSF contributions, it may be found that the subaperturing affect is significant. In this case, the grating array layout may be altered or at least separated into two 92-deg wedges as shown in Fig. 9, to maximize resolving power. The detector layout may also evolve if higher dispersion or multiple diffraction arcs are necessary to increase resolving power. Although a reasonable concept design has been presented here, it is likely to change in the lead up to Lynx. However, given its flexibility, adaptations should be readily achievable.

Acknowledgments

I would like to recognize the significant contributions that group members have made to reflection gratings and their implementation over the last several years. These members include Casey DeRoo, Ben Donovan, Fabien Grisé, Jake McCoy, Ross McCurdy, Drew Miles, Tom Peterson, Ted Schultz, James Tutt, and Ningxiao Zhang. Their contributions form the basis for this paper. I would also like to thank the terrific staff members at the Penn State Nanofabrication Lab, especially Chad Eichfeld, Michael LaBella, Guy Lavallee, Bill Drawl, and Bangzhi Liu. In addition, thanks are due to the x-ray testing support staff at the PANTER X-ray Test Facility, including Vadim Burwitz, Gisela Hartner, Carlo Pelliciari, and Marlis La Caria, as well as Eric Gullickson at the Advanced Light Source Beamline 6.3.2. Finally, I would like to thank the Lynx mission team, especially Jessica Gaskin and the ACO engineers. This work was supported by the National Aeronautics and Space Administration under Grant Nos. NNX12AI16G, NNX12AF23G, and NNX15AC42G, and internal funding from the Pennsylvania State University. The author has no relevant financial interests in the paper and no other potential conflicts of interest to disclose.

References

1. J. A. Gaskin et al., "The lynx X-ray observatory: concept study overview and status," *Proc. SPIE* **10699**, 106990N (2018).
2. F. Özel et al., "Lynx interim report," Unpublished manuscript (2018).
3. W. Cash, "Echelle spectrographs at grazing incidence," *Appl. Opt.* **21**, 710–717 (1982).
4. R. L. McEntaffer et al., "First results from a next-generation off-plane x-ray diffraction grating," *Exp. Astron.* **36**, 389–405 (2013).
5. D. M. Miles et al., "Fabrication and diffraction efficiency of a large-format, replicated x-ray reflection grating," *Astrophys. J.* **869**(95), 1–12 (2018).
6. C. T. DeRoo et al., "X-ray reflection gratings operated in an Echelle Mount," *Nat. Light Appl.* (2019) (in preparation).
7. M. J. Collon et al., "Silicon pore optics mirror module production and testing," *Proc. SPIE* **10699**, 106990Y (2018).
8. V. Burwitz et al., "AHEAD joint research activity on x-ray optics," *Proc. SPIE* **10699**, 106993T (2018).
9. C. Klauber, "Refinement of magnesium and aluminium Kα X-ray source functions," *Surf. Interface Anal.* **20**, 703–715 (1993).
10. B. D. Donovan et al., "X-ray verification of an optically aligned off-plane grating module," *Appl. Opt.* **57**, 454–464 (2018).
11. J. H. Tutt et al., "Grating alignment for the Water Recovery X-ray Rocket (WRXR)," *J. Astron. Instrum.* (2018) (in press).

Randall L. McEntaffer is a professor of astronomy and astrophysics and professor of physics at the Pennsylvania State University. He specializes in the design, fabrication, testing, and implementation of x-ray spectrographs for high throughput, high resolving power astrophysical observations. His instrumentation research topics include the fabrication of x-ray gratings using nanofabrication methodologies, alignment, and testing of aligned grating modules, and the incorporation of grating modules into space-based spectrometers.